Lithuanian Journal of Physics
Vol. **65**, No. 4, pp. 212–222 (2025)
ISSN 1648-8504 eISSN 2424-3647
DOI: https://doi.org/10.3952/physics.2025.65.4.4

IMPACT OF STRUCTURAL DESIGN AND BISMUTH SEGREGATION ON GaAsBi/GaAs QUANTUM WELLS FOR NEAR-INFRARED EMITTERS: A NUMERICAL STUDY

J. Žuvelis [a, b], A. Zelioli [a], E. Dudutienė [a], and R. Butkutė [a]

[a] *State Research Institute Center for Physical Sciences and Technology, Saulėtekio 3, 10257 Vilnius, Lithuania*
[b] *Vilnius University, Faculty of Physics, Institute of Photonics and Nanotechnology, Saulėtekio 3, 10257 Vilnius, Lithuania*
Email: justas.zuvelis@ftmc.lt

Received 8 December 2025; accepted 12 December 2025

In this work, we perform 8-band **k·p** simulations using the nextnano software to evaluate how Bi composition, quantum well width, and barrier thickness influence the interband transition energy and electron–hole envelope function overlap in GaAsBi/GaAs single- and multiple-quantum-well structures.

The results show that the optimization of Bi content, well width, or barrier thickness lead to the improved electron–hole overlap of up to approximately 10%, indicating enhanced radiative recombination efficiency. We additionally model Bi surface segregation using experimentally reported segregation probabilities and observe substantial modifications of the confinement potential, redshifts of 17–26 meV in the conduction band heavy-hole transition energy, and reductions of 5–7% in the electron–hole overlap. These effects arise from electron delocalization into Bi-enriched barriers. The study highlights that Bi segregation must be explicitly considered in the design of GaAsBi-based emitters and provides quantitative guidelines for achieving efficient and 1 μm wavelength-stable devices.

Keywords: GaAsBi, quantum wells, segregation, near-infrared, 8-band **k·p**, modelling

1. Introduction

Light-emitting diodes (LEDs) operating in the near-infrared (NIR) spectral region around 1 μm have become key components in a broad range of applications, including optical communication, remote sensing, biomedical imaging, and three-dimensional sensing systems [1, 2]. In particular, wavelengths near 980–1060 nm are widely used for fibre-coupled light sources, optical pumping of solid-state lasers, and eye-safe illumination in depth-sensing and facial recognition technologies. Achieving efficient and thermally stable NIR emission within the technologically mature GaAs platform, however, remains challenging due to the limited wavelength tunability of conventional III–V alloy systems.

InGaAs/GaAs quantum wells (QWs) currently represent the most established material system for NIR emitters on GaAs substrates, providing a good crystalline quality and well-understood growth kinetics. Yet, extending their emission beyond ~950 nm requires indium content above 25%, which induces significant compressive strain, leading to dislocation formation and degraded optical efficiency when the critical thickness is exceeded [3, 4]. Further, emission homogeneity in InGaAs/GaAs multiple quantum wells (MQWs) has been shown to deteriorate with increasing the In content due to strain accumulation and mismatch dislocations [5]. Alternatively, GaAsSb alloys offer a type-I band alignment and longer wavelength emission but suffer from a high sensitivity to growth conditions and enhanced nonradiative recombination due to Sb segregation [6, 7].

GaAsBi has emerged as a promising candidate for extending the emission wavelength of GaAs-based optoelectronic devices into the 1–1.2 μm range. Incorporation of a small fraction of Bi atoms into

GaAs leads to a substantial reduction of the bandgap energy (≈60–90 meV per % Bi) primarily through a strong modification of the valence band [8]. Moreover, the large spin–orbit splitting energy introduced by Bi suppresses non-radiative Auger recombination and intervalence-band absorption, two key mechanisms that limit efficiency in long-wavelength III–V devices [9]. These properties make GaAsBi highly attractive for the design of temperature-stable and high efficiency LEDs and laser structures operating at or beyond ~1 μm and solar cells [10, 11].

Despite these advantages, the practical implementation of GaAsBi in light-emitting structures remains hindered by challenges associated with its low-temperature growth, Bi-related surface segregation, and incorporation control [12, 13]. As a result, the experimental optimization of GaAsBi quantum wells often involves extensive trial-and-error procedures, which are time-consuming and offer a limited insight into the interplay between structural parameters and optical performance. Numerical simulation therefore could play a crucial role in guiding the design of GaAsBi-based active regions. By combining band structure modelling and quantum confinement calculations, simulations can predict transition energies, strain distributions, and carrier overlap with a high accuracy, enabling the rational optimization of well thickness, Bi composition, and barrier configuration prior to epitaxial growth [1].

To support the design of efficient GaAsBi devices, extensive modelling efforts have been undertaken to describe its highly nonlinear band-structure evolution with Bi incorporation. Atomistic tight-binding and **k·p** approaches have been developed to capture the strong valence-band anticrossing interaction and the associated giant bandgap bowing observed experimentally [8]. For instance, Usman and O'Reilly demonstrated that sp^3s^* tight-binding models reproduce the experimentally observed bandgap reduction and spin–orbit splitting by incorporating Bi-related resonant states that couple strongly to the GaAs valence band [8]. Multi-band **k·p** simulations have also been used to evaluate strain and confinement effects in GaAsBi/GaAs QWs, revealing a strong hole localization and Bi-induced band mixing that critically affect the radiative transition energy and oscillator strength [14, 15].

However, the accurate simulation of GaAsBi remains challenging due to the scarcity of experimental parameters for the hypothetical zinc-blende GaBi binary compound. Many critical quantities, including deformation potentials, band offsets, and effective masses, are not experimentally accessible and are instead estimated through interpolation or density functional theory fits [16, 17]. This uncertainty propagates into device-level simulations, making a quantitative comparison with experimental data nontrivial. Furthermore, alloy disorder and Bi clustering have a profound influence on carrier localization and transition energies, requiring atomistic supercell approaches to reproduce the broad inhomogeneous linewidths and red-shifted photoluminescence observed in experiments [14]. As a result, while modelling can provide an invaluable qualitative insight into the mechanisms governing the GaAsBi electronic structure, its employment is quite limited, and its predictive accuracy still relies heavily on experimental calibration.

In this work, we employ numerical simulations to design and optimise GaAsBi/GaAs quantum-well structures aimed at efficient emission around 1 μm. The study focuses on analyzing the influence of Bi composition, well width, and strain compensation on the electronic band structure and interband optical transitions. We also analyse the effect of previously reported Bi segregation on the transition energy in MQW systems. The results provide quantitative guidelines for achieving targeted emission wavelengths and improved radiative efficiency, offering a valuable framework for the development of next-generation GaAsBi-based NIR LEDs.

2. Methods

The electronic structures of single quantum well (SQW) and MQW structures were modelled at the Γ point using the 8-band **k·p** Schrödinger–Poisson equation solver nextnano++ [18]. One-dimensional QW simulations were performed along the [100] growth direction at 300 K. The effects of Bi content on the conduction (CB), valence (VB), and spin–orbit split-off band edges of unstrained GaAsBi were adapted from the literature [19, 20]. The Luttinger parameters of GaAsBi were taken equal to those of GaAs due to their weak composition dependence [21]. Pseudomorphic strain and its influence on the band structure were included in the calculations, with the lattice and elastic constants of GaAsBi determined by Vegard's law and the corresponding

parameters of GaAs and GaBi [22, 23]. Furthermore, the electron and hole effective masses of GaAsBi at the Γ valley were taken from the composition-dependent relations reported in Ref. [24]. Since that study showed only a negligible decrease in the effective hole mass with increasing the Bi content, it was assumed to be equal to that of GaAs.

For MQW structures, the 8-band **k·p** solver yields nearly degenerate heavy-hole-like states $|i\rangle$, each predominantly localized in a different quantum well and separated by only a small energy splitting. Because the wells are geometrically identical and the hole tunnelling probability is low due to the large effective mass of the heavy holes and the strong confinement in GaAsBi structures, these states form a quasi-degenerate subspace. In contrast, the electron effective mass is much smaller and the conduction band offset at the Γ point relative to GaAs varies less with the Bi content, resulting in a stronger interwell coupling and the formation of delocalized electron states. To evaluate interband optical transitions between the conduction-band and heavy-hole (HH) states, we construct an effective heavy-hole state as a linear combination of the quasi-degenerate HH eigenstates $|\mathrm{HH}_{\mathrm{eff}}\rangle = \Sigma_i\, c_i|i\rangle$. The real, non-negative coefficients c_i are obtained by fitting a linear combination of the corresponding block-normalized hole envelopes $\phi_i(z)$ to the electron envelope $\phi_e(z)$ using a non-negative least-squares optimization

$$\min_{c_i \geq 0} \int \left| \sum_i c_i \phi_i(z) - \phi_e(z) \right|^2 \mathrm{d}z. \tag{1}$$

The resulting effective envelope is then normalized and used to assess the maximum possible electron–hole envelope function overlap. Within the envelope-function approximation, the envelope overlap is proportional to the squared interband dipole matrix element at Γ and therefore provides a direct estimate of the relative oscillator strength and radiative recombination efficiency.

The segregation of Bi atoms during epitaxial growth was modelled using the approach proposed by Muraki et al. [25]. Although originally developed for InGaAs systems, this model has been shown to accurately reproduce the Bi surface segregation behaviour in GaAsBi structures by Luna et al. [26]. In the Muraki model, the fraction of atoms that migrate to the next monolayer during epitaxial growth is defined by the segregation probability R. The Bi content x_n inside the nth monolayer can then be expressed as

$$x_n = \begin{cases} x_0(1-R^n), 1 \leq n \leq N \text{ (well)}, \\ x_0(1-R^N)R^{n-N}, n > N \text{ (barrier)}, \end{cases} \tag{2}$$

where x_0 is the nominal bismuth content and N is the well width in monolayers. Considering that delayed Bi incorporation can be minimized through Bi pre-deposition [27], we kept the bismuth concentration inside the QW layers constant and equal to x_0, while for the barrier layers the prefactor $(1 - R^N)$ was set to unity. The dependence of Bi content on the monolayer number was further converted to spatial dependence by relating the segregation coefficient R to the effective diffusion length λ via

$$\lambda = \frac{-d}{\ln R}, \tag{3}$$

where d is half the lattice constant of the GaAs substrate. The numerical values of the segregation probability R were taken from the experimental study by Luna, which investigated GaAsBi growth by molecular beam epitaxy over a range of different substrate temperatures.

3. Results and discussion

3.1. Influence of QW composition and geometry

First, the influence of the Bi content inside the quantum wells on the transition energy between the ground-state electron and HH states, as well as on the electron–hole envelope overlap, was investigated. For those calculations, the bismuth concentration across all the wells was identical. The barrier thickness was locked to 10 nm, while the QW width was 6 nm. To illustrate the resulting band profile, Fig. 1(a) shows the band structure of a GaAsBi/GaAs MQW structure with 11% Bi at the Γ point, where the lattice mismatch between GaAsBi and GaAs gives rise to a splitting between the heavy-hole and light-hole states. The graph further depicts the electron and heavy-hole manifold wavefunction probability densities, identified by spinor projections. Even at high Bi concentrations, the electron wavefunction remains delocalized across the wells, whereas the hole-state superposition shows three distinct probability maxima, indicating only a weak coupling between the heavy-hole states (Fig. 1(b)).

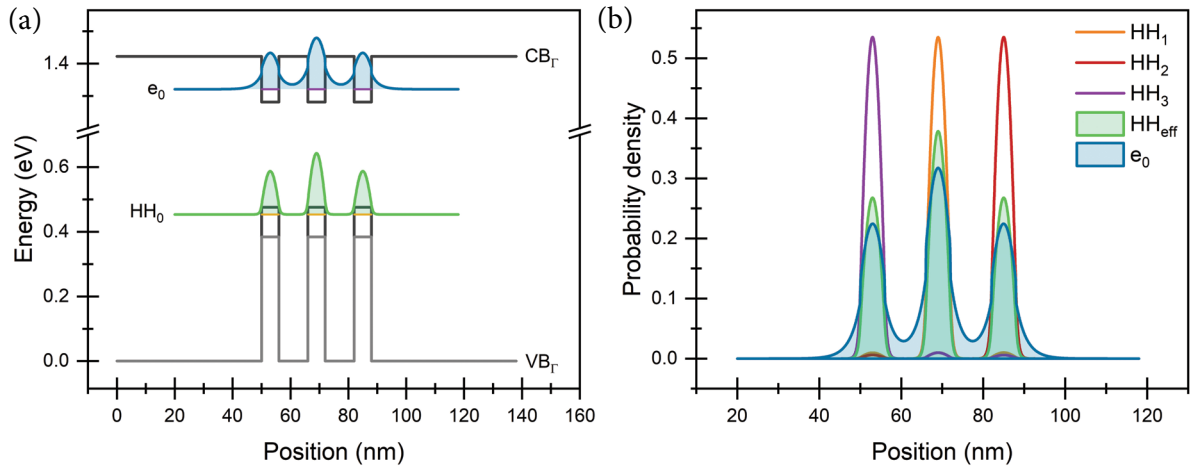

Fig. 1. (a) Band structure illustrating the conduction band (CB) and valence band (VB) edges at the Γ point, including the splitting of the heavy-hole and light-hole states. The quantized energy levels and the corresponding electron (e_0) and heavy-hole (HH_0) probability densities are shown. (b) Formation of the effective heavy-hole state relative to the electron envelope e_0 in a GaAsBi/GaAs multiple quantum-well-structure containing 11% Bi. Here, HH_i labels the near-degenerate HH states, whereas HH_{eff} denotes the calculated superposition.

The dependence of the spatial overlap on the Bi content is markedly different for the SQW and MQW structures (Fig. 2). In the MQW case, although the valence-band superposition predicts the maximum possible electron–hole envelope function overlap, the lower values obtained in the calculation reflect losses caused by electron tunnelling into the barriers. As the Bi content is increased further, interwell coupling is reduced, leading to a gradual rise in spatial envelope overlap. The difference between SQW and MQW also diminishes, indicating that the QWs begin to behave independently. The inset of Fig. 2 shows the corresponding interband transition energies between the CB and HH states. In the range of 6–12% bismuth, the model yields an almost identical linear decrease for SQW and MQW structures, with a slope of 45.2 meV per % Bi, indicating that

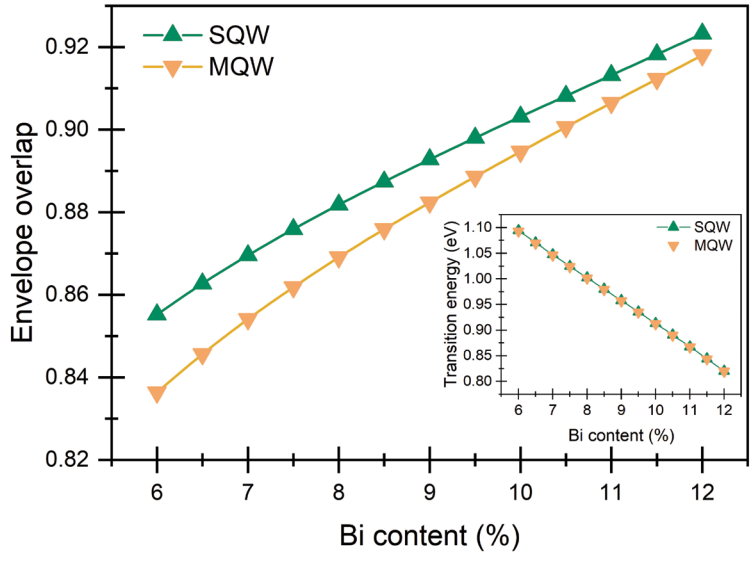

Fig. 2. The electron–hole envelope function overlap as a function of bismuth content for GaAsBi/GaAs single- and multiple-quantum-well structures. The inset shows the corresponding interband transition energies between the CB and HH states.

the effect of coupling on the CB–HH transition energy is negligible.

To evaluate the impact of barrier thickness on the interband transition properties of GaAsBi/GaAs MQW structures, the bismuth content was fixed at 7% and the QW width at 6 nm for all wells. Figure 3 shows the CB-HH transition energy (left axis) and the spatial envelope overlap (right axis) as a function of barrier thickness at the Γ point. Initially, the emission energy increases as the wells become more separated. However, once the electron and hole states become effectively decoupled and localized in individual QWs, the transition energy approaches saturation. The spatial envelope overlap between electron and hole states, on the other hand, shows an initial decrease when QWs are spaced closely together. In this range, the decrease occurs due to the decoupling of hole wavefunctions. Once barrier thickness becomes larger than 6 nm, the increase of overlap occurs due to the gradual reduction of tunnelling of the electron state and the collapse of the miniband structure.

Following the same principle, we next varied the quantum well width. As in the previous cases, the bismuth content and barrier separation were kept constant at 7% and 10 nm, respectively. The spatial envelope overlap is observed to increase with the well width (Fig. 4), as the reduced confinement energy pushes the lowest states deeper into the wells, thereby weakening the interwell coupling. Analogous to the dependence on the Bi content, the difference in overlap between SQW and MQW structures decreases as the carriers become increasingly localized within individual wells and they start to act as isolated emitters. Increasing the well width results in the decrease in the transition energy, as depicted in the inset of Fig. 4. For narrow QWs, however, the interband transition energy of the MQW structure is smaller than that of the SQW. This is primarily a result of electron coupling between identical wells, where tunnelling through the finite barriers produces a bonding-like electron ground state with energy lying slightly below the single-well level. This effect is not visible in the Bi-content dependence discussed above, because it is masked by the much stronger Bi-induced decrease of the bandgap.

3.2. Influence of Bi surface segregation and distribution

Our group has previously shown that the nextnano software package can be utilized effectively to estimate the composition and behaviour of GaAsBi based structures [28, 29]. However, the realization of GaAsBi QW devices poses many challenges, one of which is bismuth segregation

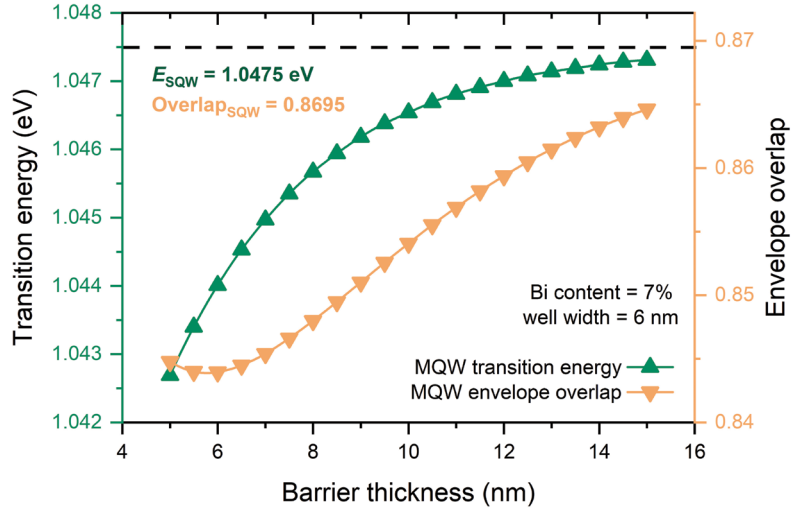

Fig. 3. Dependence of the CB–HH interband transition energy (left axis) and spatial envelope overlap (right axis) on the barrier width for 6-nm-thick GaAsBi/GaAs MQW structures with 7% bismuth. The dashed black line marks the transition energy and spatial envelope overlap for a corresponding 6-nm GaAsBi/GaAs SQW structure.

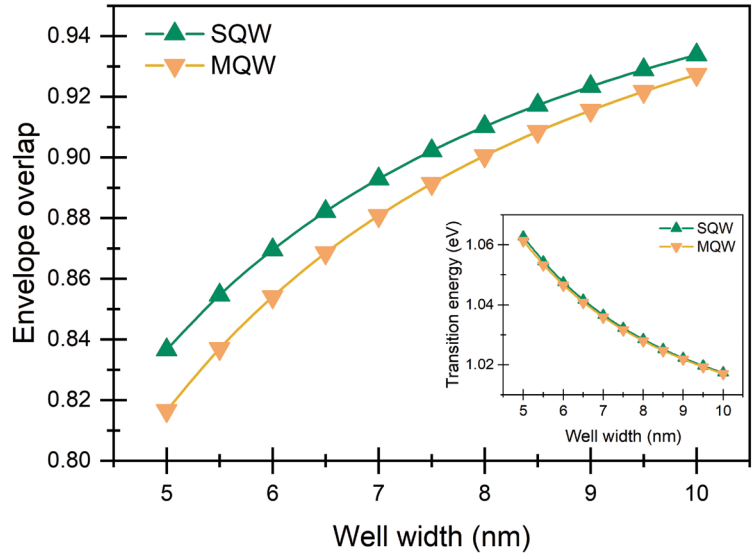

Fig. 4. Spatial envelope overlap as a function of Bi content for $GaAs_{0.93}Bi_{0.07}$/GaAs SQW and MQW structures. The inset shows the corresponding interband transition energies between the corresponding electron and HH states.

towards the surface during growth. To quantify the impact of that surface segregation on the characteristics of interband transitions, MQW GaAsBi/GaAs structures were modelled by using three sets of parameters, consisting of the surface segregation coefficient R, which denotes the probability for a Bi atom to be incorporated into the subsequently grown layer, and the maximum bismuth content x inside the QWs. In the case of $R = 0.96$, the bismuth content inside the QWs was set to 4%, consistent with the experimental results of Luna et al. [26] for GaAsBi/GaAs QW structures grown at 370°C. For the other two cases, we adopted the lower segregation probabilities $R = 0.94$ and $R = 0.9$ reported in the same study for the reduced growth temperature but increased the Bi content in the QWs to 7 and 10%, respectively. This was done to better reflect the fact that lower growth temperatures typically enable higher Bi incorporation [30]. The modelled band structures and the calculated electron and hole superposition probability densities are shown in Fig. 5(a–c). the intended well and barrier layer thickness were 6 and 10 nm, respectively.

Bi surface segregation significantly distorts the band structure and the expected carrier confinement behaviour, because bismuth incorporation into the barriers further lowers the inter-well potential barriers. Combined with the relatively weak perturbation of the conduction band, this leads to a strong coupling and delocalization of the electron states across the MQW structure. The effect is particularly pronounced in structures modelled for higher growth temperatures, i.e. those with lower Bi content and higher segregation probability (Fig. 5(a)). On the other hand, the heavy-hole states remain relatively well decoupled, owing to the large valence-band offset due to Bi incorporation, as discussed previously.

To better evaluate the effects of bismuth surface segregation on the interband transition energies and envelope overlaps, identical structures without segregation were also modelled. The results are summarized in Table 1. Compared to ideal MQW structures, bismuth segregation induces a redshift of the CB–HH transition energy. Its magnitude is on the order of tens of meV and decreases as a larger fraction of Bi is incorporated into the wells rather than the barriers. The spatial envelope overlap shows a decrease of approximately 5–7%, caused by the strong electron tunnelling into the Bi enriched barriers. Interestingly, the largest envelope misalignment was observed when $R = 0.94$ and $x = 7\%$, where the combination of substantial segregation and relatively high Bi content yields the strongest Bi enrichment of the barriers. Subsequently, the electron ground state probability density is displaced at the farthest into the barrier regions, while the hole distribution remains largely unchanged and localized.

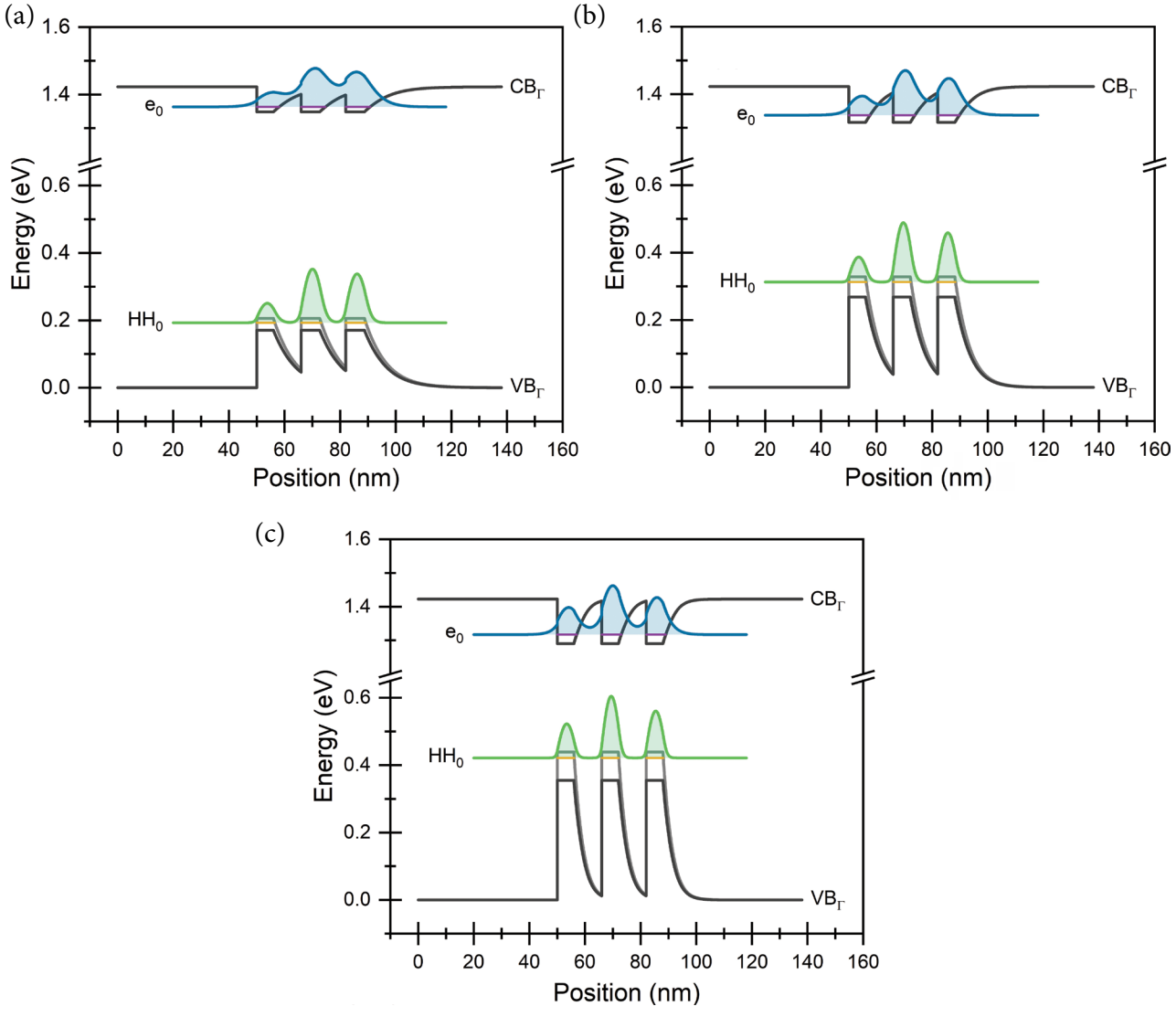

Fig. 5. Band edge profiles of 6 nm-thick GaAsBi/GaAs triple QW structures including surface segregation for (a) $R = 0.96$, $x = 4\%$; (b) $R = 0.94$, $x = 7\%$; and (c) $R = 0.90$, $x = 10\%$. Also shown are the quantized energy levels together with the electron and heavy-hole probability densities.

Table 1. Effect of Bi surface segregation on the CB–HH transition energy redshift ΔE and the reduction in the spatial envelope overlap ΔO for 6 nm-thick triple-quantum-well structures. R denotes the segregation probability coefficient and x is the Bi content in the wells.

R	x, %	ΔE, meV	ΔO, %
0.96	4	25.77	5.73
0.94	7	22.23	7.16
0.90	10	17.18	5.25

It is important to note that the calculated hole superposition states represent a best-case scenario, so the actual reduction in overlap is likely larger.

To isolate the effects of segregation on the interband transition characteristics, single-quantum-well structures were also modelled while varying the segregation coefficient R. The maximum Bi content inside the QWs was kept constant at 7%, and the intended well thickness, i.e. the width over which bismuth would be supplied, was fixed at 6 nm. We can see from Fig. 6 that the gradual elongation of the well width along the growth direction correspondingly redshifts the transition energy up to ~23 meV. In comparison, the electron–hole envelope overlap initially decreases only very weakly with increasing the segregation coefficient and only exhibits a pronounced reduction at the highest segregation probabilities. This behaviour arises

from the significantly different conduction- and valence-band offsets of GaAsBi relative to GaAs. The relatively small conduction-band offset weakly confines the electron, so that in a single QW, the Bi-enriched regions in the barriers allow the electron wavefunction to extend further into the subsequent layers along the growth direction, whereas the large valence-band offset keeps the hole state strongly localized within the well region. Recalling that during GaAsBi growth bismuth has a strong tendency to surface segregate, with segregation coefficients as high as $R = 0.96$, a careful control of growth conditions is essential to limit an excessive carrier delocalization and maintain an efficient radiative recombination.

Besides the Muraki-type segregation, the Bi profile in GaAsBi quantum wells can also be strongly inhomogeneous, either taking a triangular shape or showing an increase in the Bi content near the bottom GaAs interface [31, 32]. Although the mechanism behind these Bi distributions has not yet been clarified, their effect on interband transitions can be evaluated numerically. To this end, we modelled two rectangular GaAsBi/GaAs single quantum wells based on the experimental structures reported in Ref. [32]. The nominal well width was set to 10 nm, with a maximum Bi content of 7%. The triangular and bottom-enriched Bi distributions yield a sharp increase in the ground-state transition energy by 108 and 50 meV, respectively. Furthermore, the electron–hole envelope function overlap is observed to decrease by 18 and 4.7%, owing to the more spatially delocalized electron distribution compared with the heavy-hole state, consistent with previous observations.

4. Conclusions

In this work, we carried out a comprehensive numerical study of GaAsBi/GaAs single- and multiple-quantum-well structures to evaluate how the main design parameters such as well thickness, barrier thickness, and Bi composition influence the interband transition energies and the electron–hole spatial overlap. Using a validated set of GaAsBi material parameters compiled from multiple literature sources, our simulations yield stable and reproducible results despite the intrinsic challenges posed by the limited availability of experimental data for the GaBi binary compound.

Our results show that increasing the Bi content, QW width, or barrier thickness systematically enhances the electron–hole envelope function overlap, with improvements of up to approximately 10%. This enhancement arises from a stronger carrier localization and reduced interwell coupling in MQW

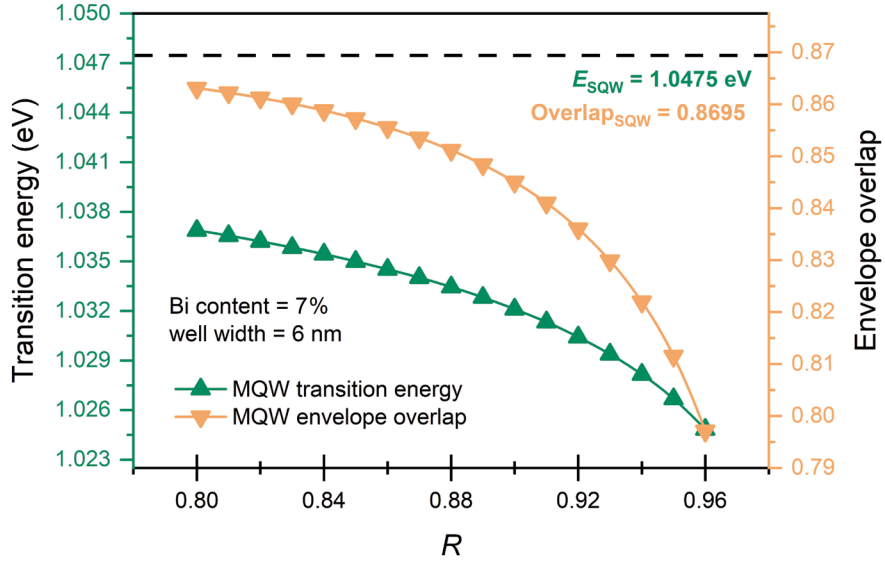

Fig. 6. CB–HH interband transition energy (left axis) and spatial envelope overlap (right axis) as functions of the Bi segregation coefficient R for 6-nm-thick GaAsBi/GaAs SQW structures. The bismuth content inside the QW region was fixed to 7%. The dashed black line marks the transition energy and spatial envelope overlap for an identical SQW without Bi segregation ($R = 0$).

structures. The dependences observed for SQW and MQW systems converge at higher Bi content and larger well and barrier widths, indicating that the wells begin to behave as independent emitters once carriers become sufficiently localized. These findings highlight that a careful selection of the geometric and compositional parameters of GaAsBi quantum wells is essential for optimizing radiative efficiency in NIR emitters.

A major practical limitation in the GaAsBi device design is the strong tendency of Bi to segregate during epitaxial growth. By incorporating experimentally reported segregation probabilities into the Muraki model, we quantified how segregation affects the structural and optical properties of MQWs. The results show that Bi incorporation into the barriers significantly distorts the potential profile, reduces the effective confinement, and leads to the pronounced delocalization of the electron wavefunction across multiple wells. Depending on the segregation coefficient, we observe redshifts of the CB–HH transition energy on the order of 17–26 meV and a reduction in electron–hole overlap of 5–7%, with the strongest misalignment occurring when a moderate segregation coincides with a relatively high intended Bi content. Simulations of SQWs further confirm that even in the absence of interwell coupling, Bi segregation reduces carrier overlap and can shift the emission wavelength by more than 20 meV. Much more pronounced effects on the interband transition characteristics are observed when the Bi distribution inside the well is strongly nonuniform. In particular, triangular and bottom-enriched Bi profiles can induce blueshifts of up to ~108 meV in the ground-state CB–HH transition energy, accompanied by a strong spatial misalignment between the electron–hole envelope functions. These changes arise from the graded band edge potential and the increased spatial delocalization of the electron wavefunction relative to the HH state and are consistent with previous experimental observations.

Overall, our findings demonstrate that Bi segregation and the nonuniform Bi distribution profiles are not secondary or negligible effects, but critical factors that directly impact the emission wavelength, electron–hole spatial overlap, and thus the radiative efficiency of GaAsBi-based devices. As a result, the accurate design of GaAsBi LED and laser structures must consider not only for the nominal well and barrier parameters but also for the effective compositional profiles created during growth, including both segregation into the GaAs barriers and nonuniform in-well distributions such as triangular profiles. These insights provide clear quantitative guidelines for the development of high-performance GaAsBi/GaAs emitters in the 1 μm spectral region and reinforce the importance of optimizing growth conditions for achieving reproducible device characteristics.

Acknowledgements

This project has received funding from the Research Council of Lithuania (LMTLT), Agreement No. S-LLT-23-3.

References

[1] R.D. Richards, N.J. Bailey, Y. Liu, T.B.O. Rockett, and A.R. Mohmad, GaAsBi: from molecular beam epitaxy growth to devices, Phys. Status Solidi B **259**(2), 2100330 (2022).

[2] T.B. Rockett, N.A. Adham, M. Carr, J.P.R. David, and R.D. Richards, GaAsBi light emitting diodes for 1050 nm broadband light sources, Proc. SPIE **PC12144**, PC121440U (2022).

[3] L.W. Sung and H.H. Lin, Highly strained 1.24-μm InGaAs/GaAs quantum-well lasers, Appl. Phys. Lett. **83**(6), 1107–1109 (2003).

[4] Y.Q. Wei, S.M. Wang, X.D. Wang, Q.X. Zhao, M. Sadeghi, I. Tångring, and A. Larsson, Long-wavelength InGaAs/GaAs quantum-well lasers grown by molecular beam epitaxy, J. Cryst. Growth **278**(1–4), 747–750 (2005).

[5] A. Zelioli, A. Špokas, B. Čechavičius, M. Talaikis, S. Stanionytė, V. Bukauskas, A. Vaitkevičius, A. Čerškus, P. Wojnar, V. Deibuk, E. Dudutienė, and R. Butkutė, Comprehensive investigation of emission homogeneity of InGaAs multiple quantum wells using spatially resolved spectroscopy, Sci. Rep. **15**(1), 32885 (2025).

[6] V. Haxha, I. Drouzas, J.M. Ulloa, M. Bozkurt, P.M. Koenraad, D.J. Mowbray, H.Y. Liu, M.J. Steer, M. Hopkinson, and M.A. Migliorato, Role of segregation in InAs/GaAs quantum dot structures capped with a GaAsSb strain-reduction layer, Phys. Rev. B **80**(16), 165334 (2009).

[7] C. Dorin, J. Mirecki Millunchick, and C. Wauchope, Intermixing and lateral composition modulation in GaAs/GaSb short period superlattices, J. Appl. Phys. **94**(3), 1667–1675 (2003).

[8] M. Usman, C.A. Broderick, Z. Batool, K. Hild, T.J.C. Hosea, S.J. Sweeney, and E.P. O'Reilly, Impact of alloy disorder on the band structure of compressively strained $GaBi_xAs_{1-x}$, Phys. Rev. B **87**(11), 115104 (2013).

[9] I.P. Marko, C.A. Broderick, S. Jin, P. Ludewig, W. Stolz, K. Volz, J.M. Rorison, E.P. O'Reilly, and S.J. Sweeney, Optical gain in GaAsBi/GaAs quantum well diode lasers, Sci. Rep. **6**(1), 28863 (2016).

[10] J. Glemža, V. Palenskis, A. Geižutis, B. Čechavičius, R. Butkutė, S. Pralgauskaitė, and J. Matukas, Low-frequency noise investigation of 1.09 μm GaAsBi laser diodes, Materials **12**(4), 673 (2019).

[11] T. Paulauskas, V. Pačebutas, V. Strazdienė, A. Geižutis, J. Devenson, M. Kamarauskas, M. Skapas, R. Kondrotas, M. Drazdys, M. Rudzikas, B. Šebeka, V. Vretenár, and A. Krotkus, Performance assessment of a triple-junction solar cell with 1.0 eV GaAsBi absorber, Discov. Nano **18**(1), 86 (2023).

[12] C.R. Tait, L. Yan, and J.M. Millunchick, Droplet induced compositional inhomogeneities in GaAsBi, Appl. Phys. Lett. **111**(4), 042105 (2017).

[13] J. Puustinen, J. Hilska, and M. Guina, Analysis of GaAsBi growth regimes in high resolution with respect to As/Ga ratio using stationary MBE growth, J. Cryst. Growth **511**, 33–41 (2019).

[14] T. Wilson, N.P. Hylton, Y. Harada, P. Pearce, D. Alonso-Álvarez, A. Mellor, R.D. Richards, J.P.R. David, and N.J. Ekins-Daukes, Assessing the nature of the distribution of localised states in bulk GaAsBi, Sci. Rep. **8**(1), 6457 (2018).

[15] I.P. Marko, P. Ludewig, Z.L. Bushell, S.R. Jin, K. Hild, Z. Batool, S. Reinhard, L. Nattermann, W. Stolz, K. Volz, and S.J. Sweeney, Physical properties and optimization of GaBiAs/(Al)GaAs based near-infrared laser diodes grown by MOVPE with up to 4.4% Bi, J. Phys. D **47**(34), 345103 (2014).

[16] H. Adamji, M. Stevens, K. Grossklaus, T.E. Vandervelde, and P. Deshlahra, Density functional theory analysis of the effect of structural configurations on the stability of GaAsBi compounds, Comput. Mater. Sci. **173**, 109401 (2020).

[17] H. Achour, S. Louhibi, B. Amrani, A. Tebboune, and N. Sekkal, Structural and electronic properties of GaAsBi, Superlattices Microstruct. **44**(2), 223–229 (2008).

[18] S. Birner, T. Zibold, T. Andlauer, T. Kubis, M. Sabathil, A. Trellakis, and P. Vogl, nextnano: general purpose 3-D simulations, IEEE Trans. Electron Devices **54**(9), 2137–2142 (2007).

[19] V. Karpus, R. Norkus, R. Butkutė, S. Stanionytė, B. Čechavičius, and A. Krotkus, THz-excitation spectroscopy technique for band-offset determination, Opt. Express **26**(26), 33807 (2018).

[20] M. Mahtab, R. Synowicki, V. Bahrami-Yekta, L.C. Bannow, S.W. Koch, R.B. Lewis, and T. Tiedje, Complex dielectric function of $GaAs_{1-x}Bi_x$ as a function of Bi content, Phys. Rev. Materials **3**(5), 054601 (2019).

[21] J. Hwang and J.D. Phillips, Band structure of strain-balanced GaAsBi/GaAsN superlattices on GaAs, Phys. Rev. B **83**(19), 195327 (2011).

[22] A. Janotti, S.-H. Wei, and S.B. Zhang, Theoretical study of the effects of isovalent coalloying of Bi and N in GaAs, Phys. Rev. B **65**(11), 115203 (2002).

[23] M. Ferhat and A. Zaoui, Structural and electronic properties of III–V bismuth compounds, Phys. Rev. B **73**(11), 115107 (2006).

[24] M. Mbarki and A. Rebey, First-principles calculation of the physical properties of $GaAs_{1-x}Bi_x$ alloys, Semicond. Sci. Technol. **26**(10), 105020 (2011).

[25] K. Muraki, S. Fukatsu, Y. Shiraki, and R. Ito, Surface segregation of In atoms during molecular beam epitaxy and its influence on the energy levels in InGaAs/GaAs quantum wells, Appl. Phys. Lett. **61**(5), 557–559 (1992).

[26] E. Luna, M. Wu, M. Hanke, J. Puustinen, M. Guina, and A. Trampert, Spontaneous formation of three-dimensionally ordered Bi-rich nanostructures within $GaAs_{1-x}Bi_x$/GaAs quantum wells, Nanotechnology **27**(32), 325603 (2016)

[27] P. Ludewig, N. Knaub, W. Stolz, and K. Volz, MOVPE growth of Ga(AsBi)/GaAs multi

quantum well structures, J. Cryst. Growth **370**, 186–190 (2013).

[28] E. Dudutienė, A. Jasinskas, B. Čechavičius, R. Nedzinskas, M. Jokubauskaitė, A. Bičiūnas, V. Bukauskas, G. Valušis, and R. Butkutė, Photoluminescence properties of GaAsBi single quantum wells with 10% of Bi, Lith. J. Phys. **61**(2), 142–150 (2021).

[29] A. Špokas, A. Zelioli, A. Bičiūnas, B. Čechavičius, J. Glemža, S. Pralgauskaitė, M. Kamarauskas, V. Bukauskas, J. Spigulis, Y.-J. Chiu, J. Matukas, and R. Butkutė, Optimising (Al, Ga) (As, Bi) quantum well laser structures for reflectance mode pulse oximetry, Micromachines **16**(5), 506 (2025).

[30] R.B. Lewis, M. Masnadi-Shirazi, and T. Tiedje, Growth of high Bi concentration $GaAs_{1-x}Bi_x$ by molecular beam epitaxy, Appl. Phys. Lett. **101**(8), 082112 (2012).

[31] S. Pūkienė, M. Karaliūnas, A. Jasinskas, E. Dudutienė, B. Čechavičius, J. Devenson, R. Butkutė, A. Udal, and G. Valušis, Enhancement of photoluminescence of GaAsBi quantum wells by parabolic design of AlGaAs barriers, Nanotechnology **30**(45), 455001 (2019).

[32] M. Skapas, E. Luna, S. Stanionytė, K. Graser, and R. Butkutė, In situ TEM study of size-controlled Bi quantum dots in an annealed GaAsBi/AlAs multiple quantum well structure, ACS Omega **10**(10), 10432–10437 (2025).

ARTIMOJO INFRARAUDONOJO RUOŽO SPINDUOLIAMS SKIRTŲ GaAsBi/GaAs KVANTINIŲ DUOBIŲ STRUKTŪRINIO DIZAINO IR BISMUTO SEGREGACIJOS SKAITMENINIS MODELIAVIMAS

J. Žuvelis [a, b], A. Zelioli [a], E. Dudutienė [a], R. Butkutė [a]

[a] *Valstybinis mokslinių tyrimų institutas Fizinių ir technologijos mokslų centras, Vilnius, Lietuva*

[b] *Vilniaus universiteto Fizikos fakulteto Fotonikos ir nanotechnologijų institutas, Vilnius, Lietuva*

Santrauka

Šiame darbe, naudojant programinį paketą *nextnano*, buvo atliktos 8 juostų **k**·**p** metodo simuliacijos, siekiant įvertinti Bi koncentracijos, kvantinių duobių pločio ir barjerinių sluoksnių storio įtaką optinių šuolių energijai bei elektronų ir skylių banginių funkcijų persiklojimui pavienių ir daugybinių GaAsBi/GaAs kvantinių duobių struktūrose.

Nustatyta, kad optimizavus įterpto Bi kiekį, kvantinių duobių plotį ir barjerinių sluoksnių storį, elektronų ir skylių sanklotą, kuri lemia spindulinės rekombinacijos našumą, galima padidinti daugiau nei 10 %. Taip pat buvo įvertinta Bi segregacijos įtaka juostinei struktūrai. Nustatyta, kad bismuto įsiterpimas į barjerinius GaAs sluoksnius lemia 17–26 meV šuolio energijos poslinkį į raudonąją pusę bei akivaizdų elektronų ir skylių banginių funkcijų sanklotos sumažėjimą (5–7 %). Šiuo tyrimu parodyta, kad bismuto segregacija yra reikšminga ir ją būtina įskaityti kuriant GaAsBi/GaAs kvantinių duobių pagrindu veikiančius spinduolius. Taip pat darbe nubrėžtos dizaino gairės, skirtos prietaisų optimizavimui efektyviai 1 μm emisijai užtikrinti.